



Deagglomeration of cohesive particles by turbulence

Yuan Yao^{1,†} and Jesse Capecelatro^{1,2}

¹Department of Mechanical Engineering, University of Michigan, Ann Arbor, MI 48109-2125, USA

²Department of Aerospace Engineering, University of Michigan, Ann Arbor, MI 48109-2125, USA

(Received 29 July 2020; revised 25 September 2020; accepted 9 November 2020)

We present a numerical study analysing the breakup of a single cohesive particle aggregate in turbulence. Solid particles with diameters smaller than the Kolmogorov length scale ($d_p < \eta$) are initially aggregated into a spherical ‘clump’ of diameter $D > \eta$ and placed in homogeneous isotropic turbulence. Parameters are chosen relevant to dust or powder suspended in air such that cohesion due to van der Waals is important. Simulations are performed using an Eulerian–Lagrangian framework that models two-way coupling between the fluid and solid phases and resolves particle–particle interactions. Aggregate breakup is investigated for different adhesion numbers Ad , Taylor microscale Reynolds numbers Re_λ and non-dimensional clump sizes D/d_p . The intermittency of turbulence is found to play a key role on the early stage breakup process, which can be characterized by a turbulent adhesion number Ad_η that relates the potential energy of the van der Waals force to turbulent shear stresses. A scaling analysis shows that the time rate of breakup for each case collapses when scaled by Ad_η and an aggregate Reynolds number proportional to D . A phenomenological model of the breakup process is proposed that acts as a granular counterpart to the Taylor analogy breakup (TAB) model commonly used for droplet breakup. Such a model is useful for predicting particle breakup in coarse-grained simulation frameworks, such as Reynolds-averaged Navier–Stokes, where relevant spatial and temporal scales are not resolved.

Key words: breakup/coalescence, particle/fluid flow, low-dimensional models

1. Introduction

The transport and deposition of tiny (cohesive) particles in turbulent flows play important roles in many engineering, environmental and medical systems. Examples include dry

† Email address for correspondence: yyaoaa@umich.edu

© The Author(s), 2021. Published by Cambridge University Press. This is an Open Access article, distributed under the terms of the Creative Commons Attribution licence (<http://creativecommons.org/licenses/by/4.0/>), which permits unrestricted re-use, distribution, and reproduction in any medium, provided the original work is properly cited.

powder inhalers for drug delivery (Begat *et al.* 2004; Yang, Wu & Adams 2013, 2015), dust ingestion in gas turbine engines (Batcho *et al.* 1987; Dunn, Baran & Miatech 1996; Bons, Prenter & Whitaker 2017; Sacco *et al.* 2018) and fluidized bed reactors (Mikami, Kamiya & Horio 1998; van der Hoef *et al.* 2008; Mahecha-Botero *et al.* 2009; Pan *et al.* 2016). Micrometre-sized particles tend to form aggregates owing to inter-particle cohesion. The dynamical evolution and morphology of these aggregates involve a complex interplay between turbulent stresses and inter-particle cohesive forces. As a result, particle clumping can arise under various circumstances, which is known to compromise the performance of the aforementioned systems. For example, agglomeration has been shown to significantly deteriorate the delivery efficiency of drug particles (Begat *et al.* 2004), accelerate turbine blade erosion in gas turbine engines (Grant & Tabakoff 1975; Hamed, Tabakoff & Wenglarz 2006) and defluidize two-phase reactors (Mikami *et al.* 1998; Cocco *et al.* 2010). Of particular interest to the present study is turbulence-induced breakup of fine particulate aggregates.

Several mechanisms are responsible for particle deagglomeration in a flow field. Breakup can be induced by inertial stresses (Kousaka *et al.* 1979; Higashitani, Iimura & Sanda 2001), rotary stresses (Sonntag & Russel 1987; Jarvis *et al.* 2005; Fanelli, Feke & Manas-Zloczower 2006a,b; Zeidan *et al.* 2007; Mousel & Marshall 2010) or turbulent stresses (Bache 2004; Wengeler & Nirschl 2007; Bähler, Morbidelli & Baldyga 2008; Weiler *et al.* 2010). Several models have recently been developed for deagglomeration due to rotary stress in simple shear flows (Dizaji, Marshall & Grant 2019; Ruan, Chen & Li 2020; Vo *et al.* 2020). The mechanisms responsible for deagglomeration in turbulence, however, are more complicated and less established. Weiler *et al.* (2010) developed a model of critical shear stress for instantaneous breakage as a function of aggregate size and the mean cohesive force. However, aggregates often break up progressively from the surface, and the critical stress at the vicinity of the aggregate is not always directly available, especially in course-grained simulations where subgrid-scale stresses are not resolved such as in Reynolds-averaged Navier–Stokes (RANS) frameworks.

The major challenge in numerically investigating the breakage of cohesive particles is properly resolving the wide range of length and time scales at play. One common approach is to couple Lagrangian particle tracking with a mean flow field obtained from RANS. The turbulent dispersion of particles is often modelled in a stochastic manner. This approach has been widely used for particle ingestion in gas turbine engines (Grant & Tabakoff 1975; Hamed *et al.* 2006; Bons *et al.* 2017). Despite its low computational cost, Lagrangian particle tracking coupled with RANS has been shown to under-predict turbulent dispersion and deposition of particles compared with experiments (Whitaker, Prenter & Bons 2015), especially near boundary layers (Rybalko, Loth & Lankford 2012; Forsyth, Gillespie & McGilvray 2018). In contrast, particle-resolved direct numerical simulation (PR-DNS) has been applied to fully capture the flow field and particle interactions (Uhlmann 2008; Vowinkel *et al.* 2019a,b). While PR-DNS is highly accurate, it is limited to small physical systems owing to its high computational cost.

Alternatively, the Eulerian–Lagrangian method tracks individual particles and solves the fluid phase on an Eulerian mesh with grid spacing larger than the particle diameter. It is capable of capturing detailed particle–particle interactions and particle–fluid coupling with moderate computational cost. This approach has been widely applied to study cohesive particles in turbulence (Ho & Sommerfeld 2002; Kosinski & Hoffmann 2010; Breuer & Almohammed 2015; Liu & Hrenya 2018; Sun, Xiao & Sun 2018; Yao & Capecelatro 2018). However, most existing studies consider one-way coupling without considering the influences of drag or volume displacement by particles on the fluid. Such an approach is not appropriate when modelling large particle aggregates as it over-predicts

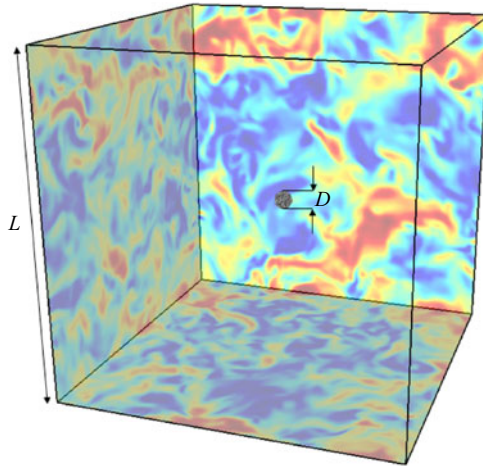


Figure 1. Simulation configuration shown with background fluid velocity (blue, low; red, high). Particles are initially close-packed in a spherical aggregate of diameter D . Particles are fixed in place until the flow reach a statistically stationary state prior to deagglomeration.

the interphase slip velocity in the vicinity of the particles (Dizaji & Marshall 2017). Another known deficiency of this method when dealing with cohesive particles is the restrictive time step.

In the present study, an Eulerian–Lagrangian framework is employed where two-way coupling is accounted for via drag and volume displacement effects. The van der Waals force model is modified to allow for soft-sphere contact. A multiscale time-stepping algorithm is introduced to minimize the computational cost. Details on the numerical framework are presented in § 2. The relative importance of turbulence and adhesion on breakup dynamics of a single aggregate is analysed by adjusting the Taylor microscale Reynolds number, Re_λ , and the adhesion number, Ad , that relates the van der Waals surface energy, γ , and the kinetic energy of particles (Marshall & Li 2014). The Hamaker constant A is varied by three orders of magnitude to mimic weakly cohesive particles (e.g. silica) and strongly cohesive materials such as metal oxides. The role of turbulence intermittency on the early stage deagglomeration is discussed. We then report the temporal evolution of the aggregate, present a breakage regime diagram and a scaling analysis of the breakup rate in § 3. Finally, a phenomenological model of the breakup process is proposed in § 4 using a mass–spring–damper analogy. Together with the scaling analysis, the proposed model provides a complete prediction of the deagglomeration process using quantities available in coarse-grained simulations that do not resolve the relevant fluid and particle time scales, such as in RANS.

In the remainder of the text, the term ‘clump’ and ‘aggregate’ will be used interchangeably.

2. Numerical configuration

2.1. Problem set-up

In this work, we consider an initially spherical ‘clump’ of particles suspended in homogeneous isotropic turbulence (see figure 1). Particles are monodisperse with diameters $d_p = 20 \mu\text{m}$ and particle-to-fluid density ratio $\rho_p/\rho = 2200$, corresponding to typical Geldart A/C-type particles (e.g. dust or powder in air) in which inter-particle

Physical parameters				
d_p	Particle diameter	20 μm		
D	Aggregate diameter	200 μm	400 μm	
N_p	Number of particles	682	5484	
ρ_p	Particle density	2650 kg m^{-3}		
ρ	Fluid density	1.2 kg m^{-3}		
ν	Fluid kinematic viscosity	$1.5 \times 10^{-5} \text{ m}^2 \text{ s}^{-1}$		
e	Coefficient of restitution	0.9		
A	Hamaker constant	$[0.4, 300] \times 10^{-20} \text{ J}$		
Non-dimensional parameters				
N^3	Number of grid points	32 ³	64 ³	128 ³
Re_λ	Taylor microscale Reynolds number	30	43	64
d_p/η	Normalized particle diameter	0.19	0.42	0.80
D/η	Normalized aggregate size	[1.9, 16]		
Ad	Adhesion number	[0, 9.0]		

Table 1. Parameters used in the simulations with square brackets denoting the parameter range.

cohesion is important (McCave 1984; Wang, Zhu & Beeckmans 2000). The simulation domain is triply periodic with sides of length $L = 400d_p$. The initial aggregate is formed by randomly distributing particles throughout the domain and assigning inward-facing normal velocities, commonly referred to as the ‘centripetal packing method’ (Liu, Zhang & Yu 1999; Yang *et al.* 2015; Ruan *et al.* 2020). First, particles are initially randomly distributed within in a spherical region without overlap. A constant centripetal force is then imposed on each particle to attract the particles towards the center of the domain. Particles undergo collisions and agglomerate in the absence of fluid forces until a single aggregate is formed. The aggregate is then submerged in the flow and held in place until a statistical stationary state is reached. At $t = 0$ the particles are free to evolve, potentially resulting in breakup and the formation of smaller aggregates, sometimes referred to as ‘flocs’ in liquid suspensions (Pandya & Spielman 1983; Flesch, Spicer & Pratsinis 1999; Jarvis *et al.* 2005; Vowinckel *et al.* 2019a; Zhao *et al.* 2020).

The competition between turbulent shear stress and inter-particle cohesion on the breakup process is studied by adjusting the initial aggregate diameter D , the Hamaker constant A and Taylor Reynolds number $Re_\lambda = u_{rms}\lambda/\nu$ where ν is the kinematic viscosity, u_{rms} is the average root-mean-square velocity and $\lambda = \sqrt{15\nu/\epsilon}u_{rms}$ is the Taylor microscale with ϵ the viscous dissipation rate. The particle adhesion number is introduced to quantify the effect of van der Waals attraction, defined as $Ad = 2\gamma/(\rho_p u_{rms}^2 d_p)$ where $\gamma = A/(24\pi\delta^2)$ is the potential energy associated with van der Waals force with $\delta = 0.165 \text{ nm}$ (Marshall & Li 2014). The Hamaker constant A is a material property that indicates the strength of cohesion due to van der Waals (Hamaker 1937). In this study, A is varied between $\mathcal{O}(10^{-21}) \text{ J}$ for weakly cohesive particles (e.g. silica) and $\mathcal{O}(10^{-18}) \text{ J}$ for strongly cohesive materials such as metal oxides (Marshall & Li 2014). A list of relevant two-phase flow parameters used in each case is provided in table 1.

2.2. Gas-phase equations

Despite the relatively small size of the particles ($d_p < \eta$), two-way coupling between the phases must be taken into account because particles are initially close-packed within an aggregate of size $D > \eta$. To account for the presence of particles without requiring a

resolution sufficient to resolve the boundary layers at the surface of each particle, a volume filter is applied to the constant-density Navier–Stokes equations (Anderson & Jackson 1967), thereby replacing the point variables (fluid velocity, pressure, etc.) by smoother, locally filtered fields. The volume-filtered conservation equations for a constant-density fluid are given by

$$\frac{\partial \alpha}{\partial t} + \nabla \cdot (\alpha \mathbf{u}) = 0, \quad (2.1)$$

and

$$\frac{\partial \alpha \mathbf{u}}{\partial t} + \nabla \cdot (\alpha \mathbf{u} \otimes \mathbf{u}) = \nabla \cdot \boldsymbol{\tau} + \mathbf{F}_{inter} + \mathbf{F}_t, \quad (2.2)$$

where \mathbf{u} is the fluid velocity, α is the fluid volume fraction and $\boldsymbol{\tau} = -p/\rho \mathbf{I} + \nu(\nabla \mathbf{u} + \nabla \mathbf{u}^\top - \frac{2}{3}(\nabla \cdot \mathbf{u})\mathbf{I})$ is the stress tensor with p the fluid-phase pressure and \mathbf{I} the identity matrix. Here \mathbf{F}_{inter} is the interphase exchange term owing to particles that is defined in § 2.4 and \mathbf{F}_t is a linear forcing term to enforce statistically stationary turbulence. It is important to note that most standard forcing techniques are not sufficient at maintaining desired turbulence properties (e.g. Re_λ) when two-way coupling is present (Mallouppas, George & van Wachem 2013). In this work, we propose to extend the linear forcing scheme of Lundgren (2003), such that the mean interphase exchange contribution is removed and the turbulence statistics remain unaffected by the presence of particles, given by

$$\mathbf{F}_t = Q_t (\alpha \mathbf{u} - \langle \alpha \mathbf{u} \rangle) - \langle \mathbf{F}_{inter} \rangle, \quad (2.3)$$

where Q_t is the linear forcing coefficient, and $\langle \cdot \rangle$ denotes the volumetric mean of the quantity within the computational domain.

The equations are implemented in the framework of NGA (Desjardins *et al.* 2008), a fully conservative solver tailored for turbulent flow computations. The Navier–Stokes equations are solved on a staggered grid with second-order spatial accuracy for both the convective and viscous terms, and the second-order accurate semi-implicit Crank–Nicolson scheme of Pierce (2001) is used for time advancement.

2.3. Particle-phase equations

Particles are treated in a Lagrangian manner where the translational and rotational motion of an individual particle i is given by

$$\frac{d\mathbf{x}_p^{(i)}}{dt} = \mathbf{v}_p^{(i)}, \quad (2.4)$$

$$m_p \frac{d\mathbf{v}_p^{(i)}}{dt} = \mathbf{f}_{inter}^{(i)} + \mathbf{f}_{col}^{(i)} + \mathbf{f}_{vw}^{(i)}, \quad (2.5)$$

and

$$I_p \frac{d\boldsymbol{\omega}_p^{(i)}}{dt} = \sum_j \frac{d_p}{2} \mathbf{n}_{ij} \times \mathbf{f}_{i,j \rightarrow i}^{col}, \quad (2.6)$$

where $\mathbf{x}_p^{(i)}$, $\mathbf{v}_p^{(i)}$ and $\boldsymbol{\omega}_p^{(i)}$ are the instantaneous particle position, velocity and angular velocity, respectively, $m_p = \rho_p \pi d_p^3/6$ is the particle mass, $I_p = m_p d_p^2/10$ is the moment of inertia for a sphere and \mathbf{n}_{ij} is the unit normal vector outward from particle i to particle j . The translational motion of each particle is determined by momentum exchange with the gas

phase, $f_{inter}^{(i)}$, which is defined in § 2.4, in addition to inter-particle collisions $f_{col}^{(i)}$ and van der Waals attraction $f_{vw}^{(i)}$, which will be made explicit in the following sections. Particle rotation is a consequence of the tangential component of the collision force, $f_{i,j \rightarrow i}^{col}$.

Owing to the large density ratio under consideration ($\rho_p/\rho = 2200$), the effects of fluid torque and lubrication forces on particle motion are neglected. In addition, it is important to note that cohesion due to van der Waals attraction and collisions are treated independently, which implicitly assumes these effects are additive in nature according to the Derjaguin, Muller and Toporov (DMT) theory (Derjaguin, Muller & Toporov 1975). The underlying assumption of the DMT theory is that cohesive forces do not modify the surface profile during particle contact. Another popular contact theory proposed by Johnson, Kendall & Roberts (1971), known as the Johnson, Kendall and Roberts (JKR) theory, assumes that adhesion occurs only within the flattened contact region such that the collision force is nonlinearly coupled with the cohesion force and consequently cannot be treated as additive. As suggested by Johnson & Greenwood (1997), the DMT approximation is valid when $\lambda_T \ll 1$ (typically $\lambda_T \lesssim 0.1$) and the JKR model is valid when $\lambda_T \gg 1$ (typically $\lambda_T \gtrsim 10$), with λ_T the dimensionless Tabor parameter defined as

$$\lambda_T = \left(\frac{2d_p \gamma^2}{E_s^2 \delta^3} \right)^{1/3}, \quad (2.7)$$

where E_s is the elastic modulus of particles. For the simulations considered herein, $0.19 \leq \lambda_T \leq 0.98$, and it is therefore not immediately obvious which assumptions readily apply. To this end, a variance-based sensitivity analysis is performed in appendix A. It is found that the results reported herein are largely unaffected by the choice in contact theory. The results were also found to be insensitive to the restitution coefficient and inclusion of fluid torque. In the remainder of this work, particle contact mechanics are based on the DMT theory owing to the low values of λ_T under consideration and to be consistent with a recently proposed cohesion model that enables larger simulation timesteps (Gu, Ozel & Sundaresan 2016), which is discussed in § 2.3.2.

2.3.1. Inter-particle collisions

Particle collisions are needed to prevent unphysical overlap that may arise when attractive inter-particle forces are present (Yao & Capecelatro 2018). In this work, normal and tangential collisions are modelled using a soft-sphere approach originally proposed by Cundall & Strack (1979). When two particles come into contact, a repulsive force is created as

$$f_{n,j \rightarrow i}^{col} = \begin{cases} -k\delta_{ij}\mathbf{n}_{ij} - \zeta\mathbf{v}_{ij,n} & \text{if } s < 0, \\ 0 & \text{else,} \end{cases} \quad (2.8)$$

where s is the distance between the particle surfaces, δ_{ij} is the overlap between the particles, \mathbf{n}_{ij} is the unit normal vector from particle i to particle j and $\mathbf{v}_{ij,n}$ is the normal relative velocity between particles i and j . The spring stiffness and damping parameter are given by k and ζ , respectively. A model for the damping parameter (Cundall & Strack 1979) uses a coefficient of restitution $0 < e < 1$ such that

$$\zeta = -2 \ln e \frac{\sqrt{km_p/2}}{\sqrt{\pi^2 + (\ln e)^2}}. \quad (2.9)$$

The spring stiffness is related to the collision time, τ_{col} , according to

$$k = m_p / 2\tau_{col}^2 (\pi^2 + (\ln e)^2). \quad (2.10)$$

Collisions are treated as inelastic with a coefficient of restitution $e = 0.9$, representative of many solid spherical objects in dry air. To properly resolve the collisions without requiring an excessively small timestep, τ_{col} is set to be 20 times the simulation time step Δt for all simulations presented in this work. A detailed account on the sensitivity of the results reported herein to the collision parameters is provided in [appendix A](#).

To account for friction between particles and, thus, particle rotation, the static friction model is employed for the tangential component of the collision force, given by

$$\mathbf{f}_{t,j \rightarrow i}^{col} = -\mu_f \left| \mathbf{f}_{n,j \rightarrow i}^{col} \right| \mathbf{t}_{ij}, \quad (2.11)$$

where $\mu_f = 0.1$ is the coefficient of friction and \mathbf{t}_{ij} is the tangential unit vector. Once each individual collision force is computed, the full collision force that particle i experiences can be expressed as

$$\mathbf{f}_{col}^{(i)} = \sum_{j \neq i} \left(\mathbf{f}_{n,j \rightarrow i}^{col} + \mathbf{f}_{t,j \rightarrow i}^{col} \right). \quad (2.12)$$

Further details can be found in [Capece de Almeida & Desjardins \(2013\)](#).

2.3.2. Van der Waals models compatible with soft-sphere collisions

The magnitude of the van der Waals force between two particles i and j of the same size, F_{ij}^{vw} , is modelled as ([Hamaker 1937](#))

$$F_{ij}^{vw}(A, s) = \frac{A}{6} \frac{d_p^2 (d_p + s)}{s^2 (2d_p + s)^2} \left[\frac{s (2d_p + s)}{(d_p + s)^2} - 1 \right]^2. \quad (2.13)$$

Owing to the short range nature of the van der Waals force, it is assumed that the force saturates at a minimum separation, $s_{min} = 1 \times 10^{-9}$ m and is cut off at $s_{max} = d_p/4$.

A brute-force implementation of the unmodified Hamaker model would require excessively small time steps to resolve inter-particle contact forces. As described previously, the spring stiffness k used in the soft-sphere collision model is determined based on the collision time τ_{col} according to (2.10), resulting in artificially ‘soft’ particles to enable larger time steps. A modified van der Waals model was recently proposed to be compatible with the soft-sphere collision model outlined in § 2.3.1 ([Gu et al. 2016](#)). The modification ensures the work done by the van der Waals force remains unchanged when particles overlap, such that its overall effect is insensitive to the choice of k and consequently the results remain unchanged as Δt is adjusted. This is accomplished by modifying the saturation distance and Hamaker constant when two particles are in direct contact, according to

$$\mathbf{f}_{vw}^{(i)} = -F_{vw}^{(i)} \mathbf{n}_{ij} = \begin{cases} -F_{ij}^{vw}(A, s - s_0) \mathbf{n}_{ij} & \text{for } s_{min}^s < s < s_{max} \\ -F_{ij}^{vw}(A^s, s_{min}) \mathbf{n}_{ij} & \text{for } s \leq s_{min}^s, \end{cases} \quad (2.14)$$

with $A^s = A(k/k_r)^{1/2}$ where k_r is the ‘real’ spring stiffness of the particle that would result in negligible overlap during collisions. A value of $k_r = 7000$ N m⁻¹ is used and the simulation spring stiffness k is chosen such that $k_r/k = 700$ as described in

Gu *et al.* (2016). The offset s_0 and shifted saturation distance s_{min}^s can be obtained by solving the following nonlinear equations

$$F_{vw}(\theta, s_{min}^R) = F_{vw}(1, s_{min}^s - s_0), \tag{2.15}$$

and

$$F_{vw}(1, s_{min}) \cdot s_{min} + \int_{s_{min}}^{s_{max}} F_{vw}(1, s) ds = F_{vw}(\theta, s_{min}) \cdot s_{min}^s + \int_{s_{min}^s}^{s_{max}} F_{vw}(1, s - s_0) ds. \tag{2.16}$$

A bisection method is used to solve the nonlinear system of equations as a preprocessing step prior to simulation runtime.

2.4. Two-way coupling

Particle information is projected to the mesh using a Gaussian filtering kernel \mathcal{G} with a characteristic length δ_f . The local volume fraction and interphase exchange term appearing in the fluid-phase equations (2.1)–(2.3) are evaluated as

$$\alpha = 1 - \sum_{i=1}^{N_p} \mathcal{G}(|\mathbf{x} - \mathbf{x}_p^{(i)}|) V_p, \tag{2.17}$$

and

$$\mathbf{f}_{inter} = -\frac{1}{\rho} \sum_{i=1}^{N_p} \mathcal{G}(|\mathbf{x} - \mathbf{x}_p^{(i)}|) \mathbf{f}_{inter}^{(i)}, \tag{2.18}$$

where $V_p = \pi d_p^3/6$ is the particle volume, and the momentum exchange term for particle i is given by

$$\mathbf{f}_{inter}^{(i)} = \mathbf{f}_{drag}^{(i)} + \rho V_p \nabla \cdot \boldsymbol{\tau}[\mathbf{x}_p^{(i)}], \tag{2.19}$$

which contains contributions of resolved fluid stresses at the particle location ($\boldsymbol{\tau}[\mathbf{x}_p^{(i)}]$) and unresolved stresses (i.e. drag) modelled according to

$$\frac{\mathbf{f}_{drag}^{(i)}}{m_p} = \frac{F(\alpha, Re_p)}{\tau_p} \alpha (\mathbf{u}[\mathbf{x}_p^{(i)}] - \mathbf{v}_p^{(i)}), \tag{2.20}$$

where $\mathbf{u}[\mathbf{x}_p^{(i)}]$ is the fluid velocity at the location of particle i , $Re_p = \alpha \|\mathbf{u}[\mathbf{x}_p^{(i)}] - \mathbf{v}_p^{(i)}\| d_p / \nu$ is the particle Reynolds number and $\tau_p = \rho_p d_p^2 / (18 \rho \nu)$ is the particle response time. In this work, $F(\alpha, Re_p)$ is modelled according to the dimensionless drag coefficient of Tenneneti, Garg & Subramaniam (2011) to take into account finite Reynolds number and volume fraction effects on the drag force.

In order to project the particle data to the grid in an efficient manner and ensure numerical stability, the two-step filtering approach of Capecelatro & Desjardins (2013) is employed. First the particle data is sent to the neighbouring grid points via trilinear extrapolation, the solution is then diffused such that the projection resembles a Gaussian with characteristic size of δ_f . To avoid restrictive time step constraints in the diffusion process, the latter step is solved implicitly via approximate factorization with a second-order alternating direction implicit (ADI) scheme. In this work, the

Deagglomeration of cohesive particles by turbulence

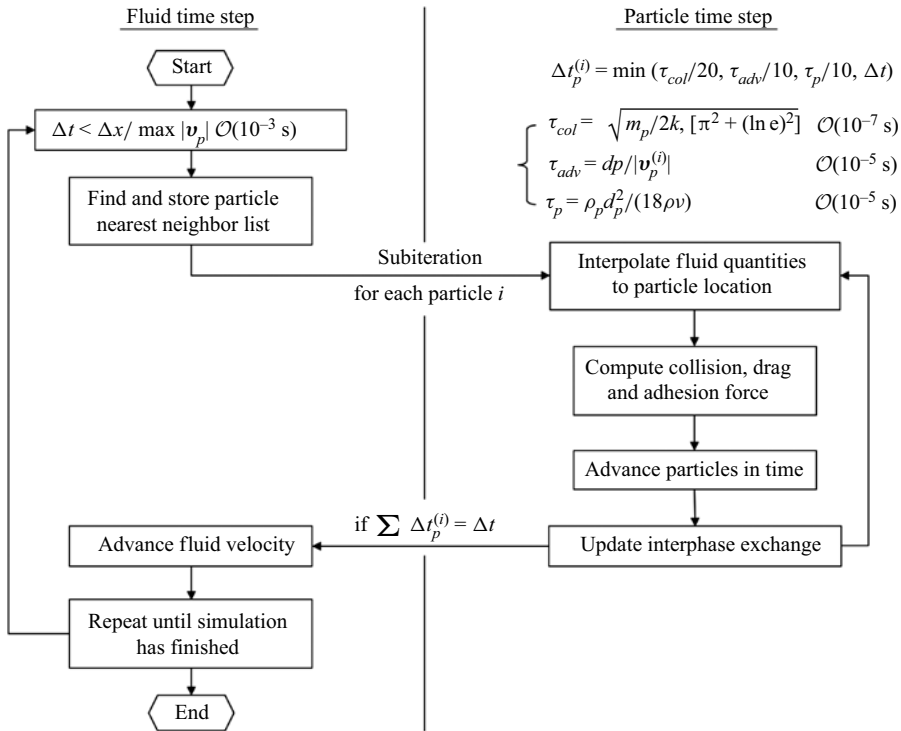


Figure 2. Multiscale time-stepping algorithm used in the simulations. For each fluid time step Δt , particles are subiterated at a smaller time step Δt_p until they are in sync with the fluid.

filter size $\delta_f = 8d_p$. Such an approach has been demonstrated to accurately predict the characteristics of particle clustering in turbulent flows (Capecelatro, Pepiot & Desjardins 2014). This simulation framework was recently demonstrated to provide accurate results when considering attractive inter-particle forces due to electrostatics (Yao & Capecelatro 2018, 2019).

2.5. Numerical time-stepping

The wide range of time scales associated with cohesive particles in turbulent flows presents a significant challenge in numerical simulations. In the present work, the fluid time scale $\tau_f = (\nu/\epsilon)^{1/2}$ is $\mathcal{O}(10^{-3} \text{ s})$, whereas the particle response time $\tau_p = \mathcal{O}(10^{-5} \text{ s})$ and the collision time scale $\tau_{col} = \mathcal{O}(10^{-7} \text{ s})$, even with the artificially softened particles and modified van der Waals model. In order to properly resolve the time scales at play in a tractable manner, a multiscale time-stepping framework based on the method proposed by Marshall (2009) is employed (see figure 2). In this approach, the fluid equations are solved on a separate time scale from the particles. To avoid $\mathcal{O}(N_p^2)$ calculations of the inter-particle forces, a nearest-neighbour detection algorithm is employed, such that interactions via collisions and van der Waals are only considered between particles in adjacent grid cells (Capecelatro & Desjardins 2013). The fluid time step, Δt , is limited by the convective time scale dictated by the Courant–Friedrichs–Lewy (CFL) number. To simplify the implementation of the two-way coupling described in § 2.4, the fluid time step is further constrained to prevent particles from moving more than one grid cell, i.e. $\Delta t < \Delta x / \max |v_p|$. This ensures that the particle nearest-neighbour list only needs to be

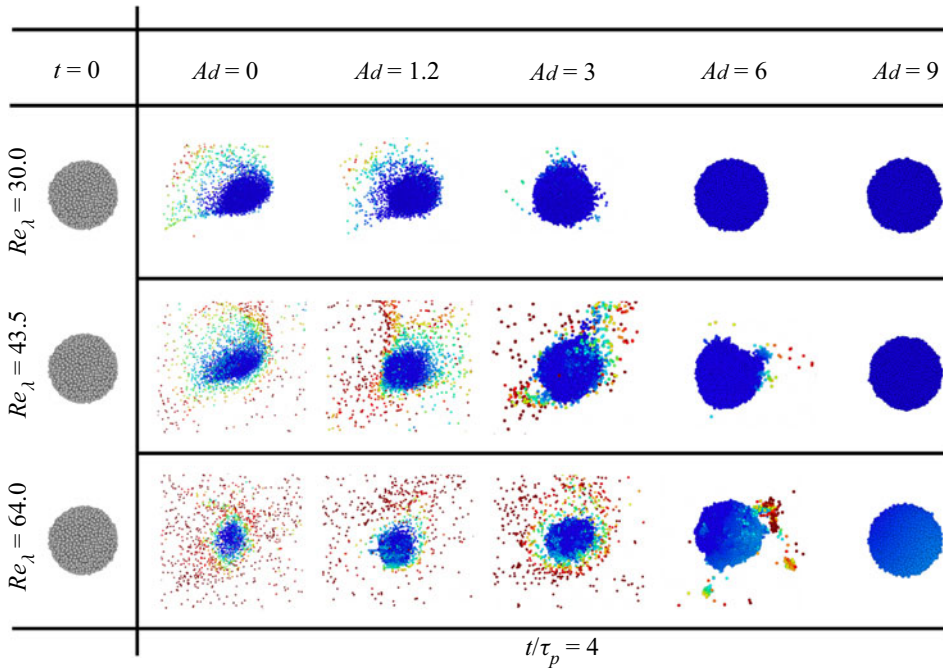


Figure 3. The first column shows an initially spherical particle aggregate ($D = 20d_p$) suspended in homogeneous isotropic turbulence. The remaining columns show particle positions after $t/\tau_p = 4$ coloured by their velocity (blue, low; red, high) for different values of Ad and Re_λ .

updated once per fluid time step. The particle advection time scale, $\tau_{adv} = d_p/|v_p|$, must be small enough to prevent significant overlap between particles. To ensure the particle dynamics are well resolved, particles are subiterated each fluid time step based on a time scale that is one order of magnitude smaller than the minimum of the collision time, particle response time and particle advection time. Finally, a second-order Runge–Kutta scheme is used for updating each particle’s position, velocity and angular velocity.

3. Results and discussion

3.1. Flow visualization

Simulations are carried out for three Taylor microscale Reynolds numbers and five adhesion numbers as listed in table 1. The spatial distribution of particles at $t/\tau_p = 4$ is compared in figure 3. In the absence of van der Waals forces, the aggregate breaks up immediately and particles are dispersed by the background turbulence. It can be observed that particles progressively shed off from the surface of the clump, and gain speed as they are transported away. Particles within the aggregate experience smaller interphase slip velocities owing to two-way coupling, resulting in negligible drag forces. It is important to note that the deagglomeration process would be markedly different if two-way coupling were not taken into account. If the simulation was performed with one-way coupling, all of the particles would experience similar drag, resulting in simultaneous breakup throughout the aggregate (see appendix A).

As Ad increases, inter-particle cohesion eventually overcomes the fluid stresses, preventing breakup from occurring when $Ad \geq 9$. For the same Ad , the rate of deagglomeration increases with increasing Re_λ due to larger fluid velocity fluctuations.

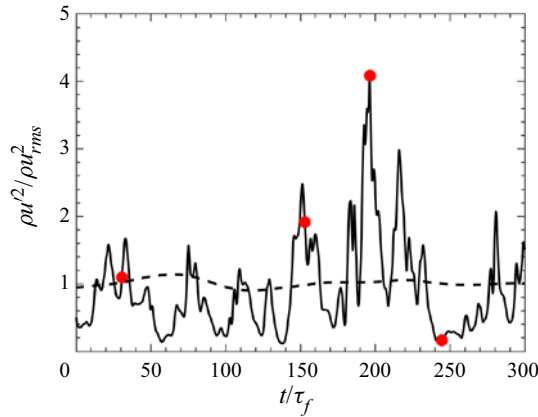


Figure 4. Instantaneous fluid stress at the aggregate surface (—) and within the entire domain (---) normalized by the root-mean-square quantities with $Re_\lambda = 30$ and $Ad = 0.3$. Four realizations under consideration (●, red).

It is clear from figure 3 that the competition between turbulent stresses acting to disintegrate the particle aggregate and cohesive forces opposing breakup is entirely controlled by Re_λ and Ad . A quantitative assessment of Re_λ and Ad on the evolution of the breakup process is presented in the following sections.

3.2. The role of turbulence intermittency on deagglomeration

Fluid stresses exerted on the aggregate surface by turbulence is highly intermittent. Figure 4 shows a comparison of the fluid stress at the aggregate surface, defined as $\rho u'^2|_c = \sum_{i=1}^{N_p} \rho \|\mathbf{u}'[\mathbf{x}_p^{(i)}]\|^2 / N_p$, with the domain-averaged stress. As can be seen, the instantaneous fluid stress at the vicinity of the aggregate fluctuates by as much as four times the domain-averaged value. The time scales of these fluctuations are significantly smaller than the time required to complete breakup ($\sim 300\tau_f$ for this case), which amplifies the effect of turbulence intermittency on early stage breakup.

To investigate the effect of turbulence intermittency on the breakup process, particles are held in place until four values of t/τ_f as highlighted in red in figure 4. The particle clump is then free to evolve from that particular instant in time. These four realizations contain different fluid stress levels at the vicinity of the clump. In order to quantify its effect on breakup, the gyration radius, R_g , and the fractal dimension, D_f , are computed, which are commonly used to characterize the dynamics and morphology of particle aggregates (Friedlander 2000; Ruan *et al.* 2020). The gyration radius is defined as

$$R_g = \sqrt{\frac{1}{N_c} \sum_{i=1}^{N_c} \|\mathbf{x}_p^{(i)} - \mathbf{x}_c\|^2}, \quad (3.1)$$

where N_c is the number of particles in the clump, $\mathbf{x}_c = \sum_{i=1}^{N_c} \mathbf{x}_p^{(i)} / N_c$ is the center of mass of the aggregate. The fractal dimension indicates the compactness of its spatial structure. For a dense spherical aggregate, $D_f \approx 3$. In this work, we follow Ruan *et al.* (2020) and obtain D_f by solving the following nonlinear equation

$$N_c = k_f (2R_g/d_p)^{D_f}, \quad (3.2)$$

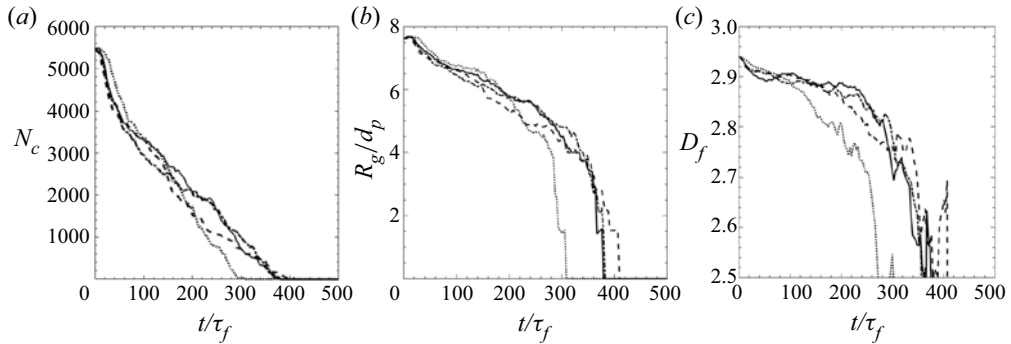


Figure 5. Characteristics of the aggregate for four different realizations with $Re_\lambda = 64$ and $Ad = 0.3$: (a) number of particles, (b) normalized Gyration radius and (c) fractal dimension of the particle clump. Line types $-$, $- \cdot -$, $---$ and \dots correspond to red data points from left to right shown in figure 4.

where the fractal prefactor k_f is

$$k_f = 0.7321 + 0.8612^{((D_f-1)/2)^{1.95}}. \tag{3.3}$$

The initial clump generated by centripetal packing has values $R_g/d_p = 7.625$ and $D_f = 2.94$. The total volume of the clump is defined by $V_c(t) = \{\mathbf{x} \in \mathbb{R}^3 : \alpha(\mathbf{x}, t) < 0.75\}$, which is evaluated at each simulation timestep in order to quantify the evolution of R_g and D_f . N_c represents the number of particle inside the volume $V_c(t)$.

Figure 5 shows the temporal evolution of N_c , R_g and D_f for the four realizations with $Re_\lambda = 64$ and $Ad = 0.3$. It can be seen that the breakup statistics change substantially over the different realizations despite Re_λ and Ad being held constant. The cases with higher initial turbulence intensity result in quicker initial breakup yet later time statistics remain relatively unchanged. This can be associated with the time scale of the intermittent fluctuations being significantly smaller than the time it takes for total breakage. Although the aggregate breaks up faster with larger initial surface stress, it is subject to smaller fluctuations on average (see figure 4) resulting in slower breakage at late times. Despite this intermittency, N_c decays in an approximately linear manner whereas R_g decreases much faster at late time. The fractal dimension D_f decreases from 2.94 to approximately 2.5, indicating significant deformation of the aggregate. Note that the statistics of the fractal dimension D_f becomes noisy when the number of particles in the aggregate is $N_c \lesssim 1000$ or equivalently the gyration radius $R_g \lesssim 2d_p$ owing to the limited sample size. To mitigate the effect of turbulence intermittency on the subsequent results reported herein, all simulations are initialized such that $\rho u^2|_c$ is approximately equal to the global fluid stress at $t = 0$.

3.3. Early stage deagglomeration

Figure 6 shows the temporal evolution of the number of particles N_c and the gyration radius R_g of the aggregate for $Re_\lambda = 64$ as a function of Ad . The number of particles within the aggregate decreases linearly as it breaks up. As Ad increases, inter-particle cohesive forces become more significant, resulting in a decreased rate of deagglomeration. It can be seen that the deagglomeration statistics exhibit a stair-step behaviour when Ad exceeds a critical value of $Ad = 3$. This is attributed to the intermittency of turbulent fluctuations, as shown in figure 7. Particles shed off from the aggregate more rapidly when the clump experiences larger velocity fluctuations. Similar trends are also observed for the gyration

Deagglomeration of cohesive particles by turbulence

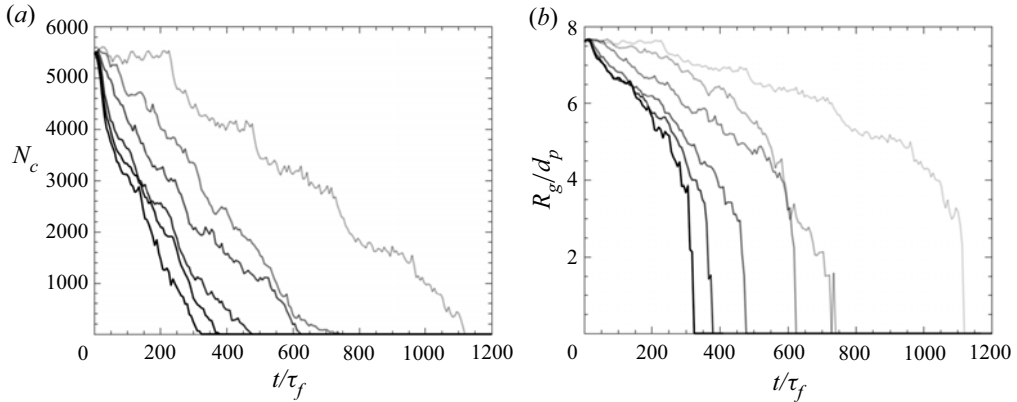


Figure 6. Temporal evolution of (a) the number of particles and (b) gyration radius of the aggregate for $Re_\lambda = 64$ and $Ad = 0, 0.3, 0.6, 1.2, 1.8, 3$ (from black to light gray).

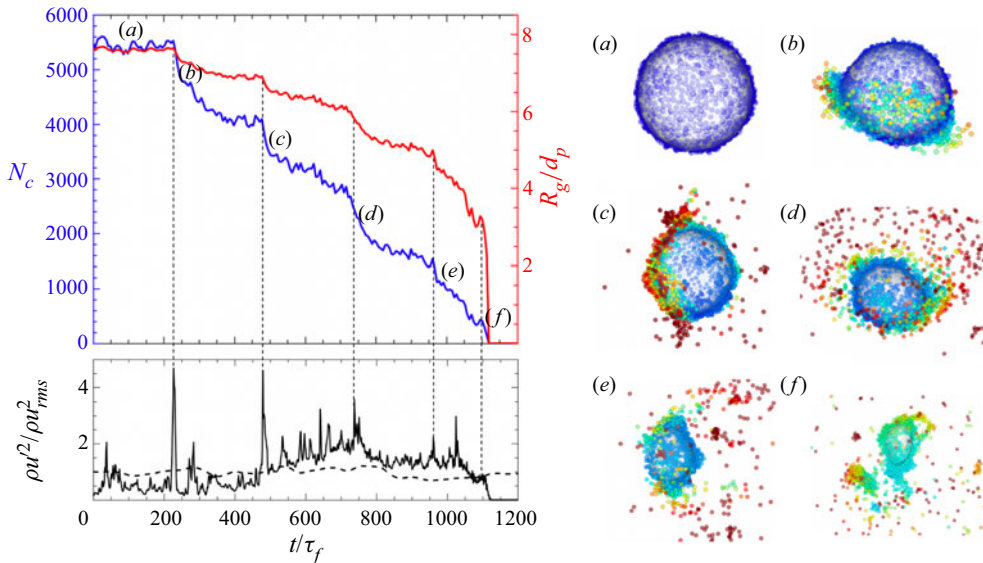


Figure 7. The plots on the left temporal evolution of the number of particles (blue) and gyration radius (red) of the aggregate and corresponding fluid stress at the aggregate surface for $Ad = 3$ and $Re_\lambda = 64$. Stair-step behaviour is observed in the statistics indicating intermediate breakup occurs when the local fluid stress exceeds a threshold value. In (a)–(f) the corresponding instantaneous snapshots of particle position are shown, with iso-contour of $\alpha = 0.75$ (white) representing the surface of the aggregate. Colour scheme is the same as figure 3.

radius, whereas the radius decreases faster during the late stage of deagglomeration, as a direct consequence of the linear decay in N_c , or equivalently linear decay in aggregate volume. Note that when $Ad > 3$, particles become so cohesive that the clump retains its original shape and size, which were omitted from figure 6.

Figure 7 highlights the effect of fluid stresses at the aggregate surface for $Ad = 3$ and $Re_\lambda = 64$. The iso-contour of $\alpha = 0.75$ shown in white is used to visualize the surface of the aggregate. A direct one-to-one correspondence can be observed between the stair-step breakup behaviour and instantaneous turbulent velocity fluctuations.

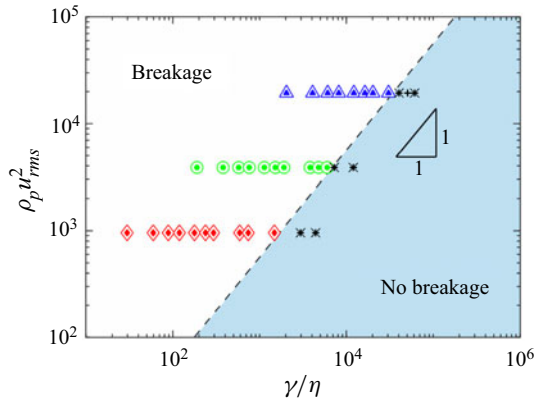


Figure 8. Breakage regime diagram for a particle aggregate suspended in homogeneous isotropic turbulence for $Re_\lambda = 30$ (◆, red), 43 (●, green), 64 (▲, blue) and non-dimensional clump size $D/d_p = 10$ (solid), 20 (hollow), with + and × denoting cases without breakage for $D/d_p = 10$ and 20, respectively. The linear dashed line separating the breakup outcome is given by $Ad_{\eta,crit} = \gamma/(\rho_p u_{rms}^2 \eta) = 1.8$.

The snapshots indicate the abrupt decrease in aggregate size is associated with turbulent eddies interacting with the aggregate resulting in breakup of smaller satellite aggregates. Before breakage, the clump is seen to remain relatively spherical. In the presence of large velocity fluctuations, the aggregate breaks from the side of its surface where the velocity gradient is high. As the aggregate shrinks, the net effect of cohesion within the aggregate also decreases and consequently breaks up in all directions. Although the surface area is smaller than the original aggregate, particles shed off at higher speeds resulting in the same rate-of-change in N_c . At late time ($t > 1000\tau_f$), D drops below a critical value where turbulent eddies can no longer break the aggregate into smaller pieces, i.e. when $D \sim \eta$.

3.4. Scaling analysis

To better understand the role of turbulence and adhesion on the breakup process, the breakage outcome associated with each simulation is plotted in terms of the adhesive stress, γ/η , and the turbulent stress, $\rho_p u_{rms}^2$. As shown in figure 8, larger fluid stress results in a transition from a ‘no breakage’ regime to a ‘breakage’ regime at a given γ/η . A simulation is classified as ‘no breakage’ when N_c remains unchanged for $t \geq 1000\tau_f$. Similarly, at a given $\rho_p u_{rms}^2$, the increase of γ/η , either due to enhanced cohesion or smaller η , reduces the likelihood of breakup. The breakup outcome is found to depend on a turbulent adhesion number $Ad_{\eta,crit} = \gamma/(\rho_p u_{rms}^2 \eta) = 1.8$ where $Ad_\eta = Ad(d_p/\eta)$. Note that for simple shear flow where η is not well defined, it has been found that the breakage outcome is instead characterized by D (Ruan *et al.* 2020). The simulations performed in the present study indicate that the characteristic length scale associated with aggregate breakup is η when $\eta \ll D$. In simple shear flow, particles experience a uniform shear rate within the aggregate, therefore larger aggregates will experience larger velocity differences across the surface. In homogeneous isotropic turbulence, however, turbulent eddies create local regions of high shear of size proportional to η . When $\eta \ll D$, these eddies are agnostic to the clump size D resulting in progressive breakup into smaller clumps, as depicted in figure 7.

Figure 6 shows that the breakup rates ($\dot{N}_c = dN_c/dt$) are approximately constant for each case under consideration. The breakup rates are extracted from each simulation and

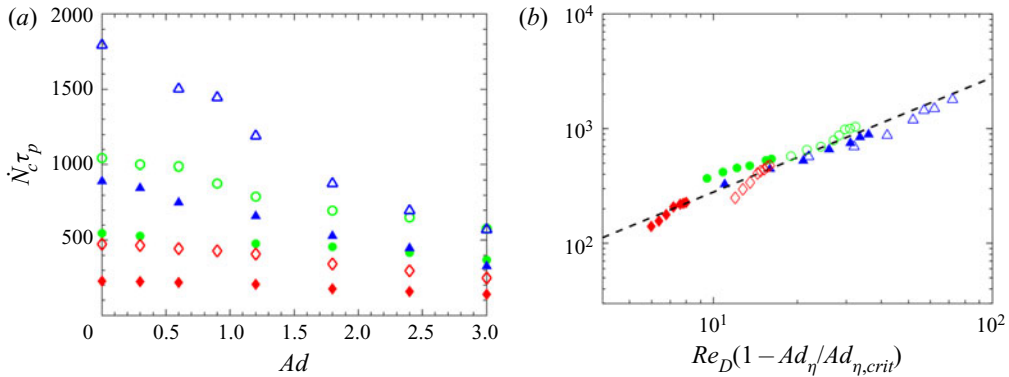


Figure 9. Rate of deagglomeration quantified by the time-rate-of-change of number of particles within the aggregate for different Ad , $Re_\lambda = 30$ (\blacklozenge , red), 43 (\bullet , green), 64 (\blacktriangle , blue) and aggregate size $D/d_p = 10$ (solid), 20 (hollow). Rate of deagglomeration plotted (a) as a function of Ad and (b) as a function of $Re_D(1 - Ad_\eta/Ad_{\eta,crit})$. Here $\dot{N}_c \tau_p = 28 Re_D(1 - Ad_\eta/Ad_{\eta,crit})$ (---).

plotted in figure 9(a). It can immediately be seen that the breakup rate increases with D and Re_λ , but decreases with Ad . The effect of D and Re_λ can be taken into account via an aggregate Reynolds number $Re_D = u_{rms}D/\nu$. When $Ad_\eta = 0$, adhesion has no effect on the breakup rate and consequently $\dot{N}_c \tau_p \sim Re_D$. When $Ad_\eta \geq Ad_{\eta,crit}$, no breakage will occur according to figure 8 ($\dot{N}_c \tau_p = 0$). With this, a correction factor $(1 - Ad_\eta/Ad_{\eta,crit})$ can be introduced to account for the effect of cohesion. Based on these observations, the data is rescaled with respect to $Re_D(1 - Ad_\eta/Ad_{\eta,crit})$. As shown in figure 9(b), the breakup rate follows a linear scaling given by $\dot{N}_c \tau_p = 28 Re_D(1 - Ad_\eta/Ad_{\eta,crit})$. Note that small deviations are observed at lower Reynolds numbers (e.g. $Re_\lambda = 30$). For these cases, the eddy size becomes comparable to D , and turbulence must break up the entire aggregate instead of a piece of it. As a result, the assumption that η is the characteristic length scale for deagglomeration does not hold at low Reynolds numbers and the breakup will exhibit dependence of D/d_p instead. Based on the simulation results, the dependence of breakup on η is applicable when $D/\eta \gtrsim 5$.

4. Phenomenological model of deagglomeration

Despite valuable insights provided by the numerical simulations presented herein and many other works using PR-DNS, they are limited to relatively small-scale systems owing to the high computational cost needed to resolve the relevant length and time scales. Particle transport in large-scale systems is typically modelled without knowledge of the velocity field at the scale of individual particles. However, the breakup of cohesive particles reported in §§ 3.2 and 3.3 are shown to depend strongly on local turbulence statistics such as η and u_{rms} . In addition, the effect of turbulence intermittency is not captured when particles traverse an averaged flow field, such as in the case of RANS. The aim here is to develop a reduced-order model capable of capturing the breakup of cohesive particles in the absence of a resolved turbulent flow field.

The Taylor analogy breakup (TAB) model is widely used in calculating droplet breakup. This method is based on Taylor's analogy (Taylor 1963) for an oscillating and distorting droplet. The droplet deformation is treated as a mass–spring–damper system, where the surface tension force acts as a restorative force, the force exerted by the

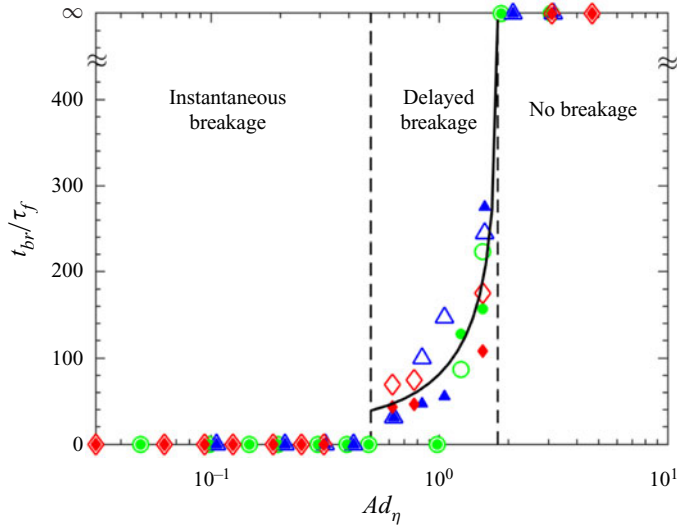


Figure 10. Time to initial breakup t_{br} as a function of the turbulent adhesion number. Symbols are the same as figure 8. The black line corresponds to (4.14) with $C_F = 0.8$, $C_k = 2 \times 10^{-4}$, $C_d = 0.3$ and $C_b = 1$. The vertical dashed lines correspond to $Ad_\eta = 0.5$ and $Ad_\eta = 1.8$.

surrounding gas phase acts as an external force, and the droplet viscosity acts as a damper. Motivated by the TAB model, we propose a similar mass–spring–damper analogy to model turbulence-induced breakup of cohesive particles. In this case, the van der Waals force is treated as an analogue to the droplet surface tension, and friction due to inter-particle contact is treated as an analogue to the droplet viscosity. We refer to this model as a granular Taylor analogy breakup (G-TAB) model.

Assuming the local turbulence statistics are known from a turbulence model such as RANS, Ad_η can be determined to estimate whether or not breakup occurs. As shown in figure 10, three distinct breakup regimes are observed: $Ad_\eta \leq 0.5$, the cohesive force is weak compared with turbulent stresses and the aggregate breaks up instantaneously; $0.5 < Ad_\eta \leq 1.8$, the competition between turbulence and cohesion results in delayed breakage of the aggregate; and when cohesion becomes significant ($Ad_\eta > 1.8$), turbulence is unable to overcome the attractive forces, resulting in no breakup. The G-TAB model is employed to predict the breakup time as a function of Ad_η when $0.5 < Ad_\eta \leq 1.8$. The governing equation is given by

$$F - kx - d \frac{dx}{dt} = m \frac{d^2x}{dt^2}, \tag{4.1}$$

where x is the displacement of the aggregate equator from its spherical (undisturbed) position. The coefficients of this equation are based on Taylor’s analogy, given as

$$\text{inertial force due to turbulence: } \frac{F}{m} = C_F \frac{\rho u_{rms}^2}{\rho_p \eta}, \tag{4.2}$$

$$\text{restorative force due to adhesion: } \frac{k}{m} = C_k \frac{\gamma}{\rho_p \eta^3}, \tag{4.3}$$

$$\text{damper due to inter-particle friction: } \frac{d}{m} = C_d \frac{\mu_p}{\rho_p \eta^2}, \tag{4.4}$$

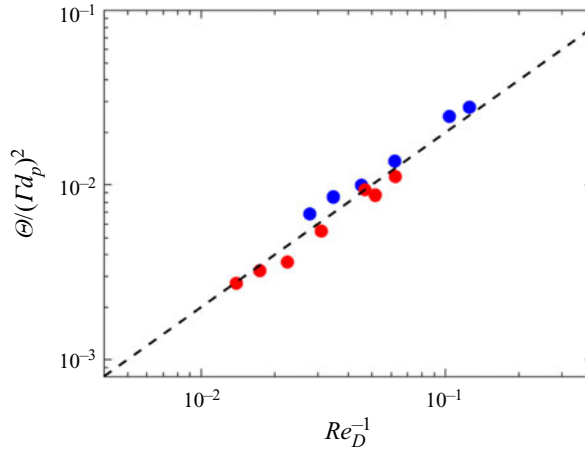


Figure 11. Scaling of the mean granular temperature within the aggregate for $D = 10d_p$ (blue) and $20d_p$ (red). Here $\Theta / (\Gamma d_p)^2 = 0.2 Re_D^{-1}$ (—).

where μ_p is the effective solids viscosity at random close packing (RCP) and C_F , C_k and C_d are model coefficients that will be determined later.

For non-cohesive particles, Bocquet *et al.* (2001) gives the solids viscosity as $\mu_p^0 = (m_p \sqrt{\Theta} / d_p^2) g_0^{\beta-1}$ from kinetic theory, where $\Theta = \langle \mathbf{v}_p^{(i)} \cdot \mathbf{v}_p^{(i)} \rangle / 3$ is the granular temperature, $g_0 = (1 - n/n_c)^{-1}$ is the radial distribution function at contact with n the local number density and n_c the maximum number density at RCP. Here $\beta = 1.75$ is a phenomenological constant measured from experiments. For cohesive particles, μ_p increases monotonically with increasing adhesion due to enhanced inter-particle attraction. A linear correction has been introduced by Roy, Luding & Weinhart (2017) as $\mu_p = \mu_p^0 (1 + 1.47 Bo)$ where $Bo = F_{vdw} / (p_s d_p^2)$ is the Bond number that measures the cohesion strength relative to the compressive force. The solids pressure p_s at RCP is given as $p_s = n_0 g_0 m_p \Theta$ with $n_0 = (1 + e)(\pi/3)n_c^2 d_p^3$ (Bocquet *et al.* 2001). Based on these relations, μ_p is computed as a function of Θ and Bo

$$\mu_p = (m_p \sqrt{\Theta} / d_p^2) g_0^{\beta-1} (1 + 1.47 Bo), \tag{4.5}$$

which depends on Re_λ and Ad . Based on the simulation results reported herein, $\Theta / (\Gamma d_p)^2$ is found to scale linearly with Re_D^{-1} (see figure 11). Therefore, we propose a simple model for the granular temperature of the particles within the aggregate near RCP as

$$\Theta = C_\Theta Re_D^{-1} (\Gamma d_p)^2, \tag{4.6}$$

where the coefficient $C_\Theta = 0.2$ is determined from the simulations, and the shear rate is approximated as $\Gamma \approx u_{rms} / D$. A more detailed algebraic expression for Θ was presented by Syamlal, Rogers & O'Brien (1993).

The aggregate is assumed to break up if the distortion grows to a critical ratio of the Kolmogorov length scale. This breakup requirement is given as

$$y = x / (C_b \eta) > 1. \tag{4.7}$$

Consequently, (4.2) can be non-dimensionalized as

$$\frac{d^2y}{dt^2} = \frac{C_F}{C_b} \frac{\rho}{\rho_p} \frac{u_{rms}^2}{\eta^2} - \frac{C_k \gamma}{\rho_p \eta^3} y - \frac{C_d \mu_p}{\rho_p \eta^2} \frac{dy}{dt}, \quad (4.8)$$

which exhibits the following analytical solution

$$y(t) = Ad_c \left(1 - e^{-(t/t_d)} \left[\cos(\omega t) + \frac{1}{\omega t_d} \sin(\omega t) \right] \right), \quad (4.9)$$

where

$$\frac{1}{t_d} = \frac{C_d}{2} \frac{\mu_p}{\rho_p \eta^2}, \quad (4.10)$$

$$Ad_c = \frac{C_F}{C_k C_b} \frac{1}{Ad_\eta} \frac{\rho_f}{\rho_p}, \quad (4.11)$$

and

$$\omega^2 = C_k \frac{\gamma}{\rho_p \eta^3} - \frac{1}{t_d^2}. \quad (4.12)$$

The aggregate is assumed to break up when the maximum displacement satisfies

$$\max(y) = Ad_c \left(e^{-\pi/(\omega t_d)} + 1 \right) > 1, \quad (4.13)$$

and the corresponding breakup time is uniquely obtained by solving

$$y(t_{br}) = 1, \quad t_{br} < \pi/\omega. \quad (4.14)$$

The model coefficients are determined by solving (4.10)–(4.12) and (4.14) using t_{br} extracted from each simulation. The G-TAB model is able to predict t_{br} and the correct $Ad_{\eta,crit}$ as shown in figure 10 with $C_F = 0.8$, $C_k = 2 \times 10^{-4}$, $C_d = 0.3$ and $C_b = 1$. These coefficients are of the same order as the original TAB model except for C_k , which is significantly smaller, indicative that a larger restorative force is required to prevent breakup compared with that of the surface tension required for liquid droplets. This discrepancy is primarily due to the short-range nature of the van der Waals force which results in non-restorative deformation as inter-particle distances increase beyond the force range. Note that the model is not applied when $Ad_\eta < 0.5$, resulting in the instantaneous breakage regime where $t_{br} = 0$.

In summary, for any spherical aggregate of particles with known size ratio D/d_p , Hamaker constant A and local turbulence quantities η and u_{rms} , the non-dimensional numbers Ad_η , Bo and Re_D can be calculated. With this, the G-TAB model predicts the time it takes to initiate breakage based on Ad_η and Bo . If an aggregate is predicted to break (i.e. $Ad_\eta < 1.8$), then the rate of breakup is modelled using the scaling shown in figure 9 given by

$$dN_c/dt = \frac{28 Re_D}{\tau_p} (1 - Ad_\eta/Ad_{\eta,crit}). \quad (4.15)$$

This provides a comprehensive prediction of the deagglomeration process of a clump of cohesive particles in turbulence from the onset of breakage to complete fragmentation into primary particles. Because u_{rms} and η are readily available in a RANS calculation, the G-TAB model can readily be incorporated. We note that this model is specifically

designed for the breakup of a single dense spherical aggregate in turbulence. Although non-spherical or less-densely packed aggregates may require different model coefficients, the mass–spring–damper analogy proposed here is anticipated to hold.

Many efforts have recently been made towards modelling aggregate breakup due to particle interactions. Chen & Li (2020) showed that the collision-induced breakage rate scales exponentially with Ad and aggregate size. van Wachem *et al.* (2020) proposed a discrete fragmentation model (DFM) to simulate the breakup behaviour due to aggregate–aggregate and aggregate–wall collisions without tracking each individual primary particle. Unlike these studies, the present work provides a framework that isolates the effect of turbulence on particle breakup using a simple phenomenological model. At present, experimental measurements of particle breakup in turbulence are scarce. While such measurements are challenging to make experimentally, primarily due to the difficulty in seeding an individual aggregate in a controlled manner and due to the opaque nature of the particles, such data would be invaluable to further validate such models.

5. Conclusion

In the present study, a ‘clump’ of Geldart A/C-type particles (e.g. dust or powder in air) was placed in homogeneous isotropic turbulence to study the interplay between turbulence and adhesion on deagglomeration. Numerical simulations were carried out in an Eulerian–Lagrangian framework that resolves particle–particle interactions and models fluid–particle coupling. The adhesion number Ad , Taylor microscale Reynolds number Re_λ and non-dimensional clump size D/d_p were varied to investigate the breakup criteria and breakup rate of the aggregate.

To fully resolve the wide range of length and time scales present in the system, we employed a multiscale time-stepping algorithm that subiterates particles at a smaller time step than the fluid phase. A modified linear-forcing technique was introduced to maintain statistically stationary turbulence in the presence of particles with two-way coupling. A modified van der Waals model developed for soft-sphere collisions was also adopted to allow for larger simulation time steps while keeping the results insensitive to the choice of particle stiffness. A variance-based sensitivity analysis was performed to quantify the relative importance of the modelling parameters appearing in the particle-phase equations on the time-to-breakup and breakup rate. The simulation results were found to be most sensitive when switching between one-way and two-way coupling. In the absence of two-way coupling, the local flow remains unmodified in the presence of particles, resulting in relatively large interphase slip velocities and consequently instantaneous breakup.

The temporal evolution of the aggregate size and flow visualizations demonstrated that turbulence intermittency plays an important role on the deagglomeration process. It was found that the time rate of breakup is affected substantially by different flow realizations of the same Re_λ . As particles become more cohesive (e.g. $Ad \geq 3$), a stair-step behaviour was observed for the breakup rate owing to the presence of large turbulent velocity fluctuations at the vicinity of the aggregate.

The aggregate is shown to breakup progressively into smaller clumps proportional to η . A regime map of fluid stress versus adhesive stress revealed that a critical turbulent adhesion number, $Ad_{\eta,crit} = \gamma / (\rho_p u_{rms}^2 \eta) = 1.8$, is capable of predicting the breakup outcome of an aggregate in turbulence. A scaling analysis further demonstrated a linear relation between the time rate of breakup \dot{N}_c and the aggregate Reynolds number Re_D , with a correction due to adhesion ($1 - Ad_\eta / Ad_{\eta,crit}$).

As a direct analogue to the TAB model commonly used for droplet breakup in the spray community, the analysis performed herein was used to inform a mass–spring–damper model to predict the breakup time of the aggregate, referred to as G-TAB. Here, turbulent velocity fluctuations act to deform the aggregate, damped by solid-phase shear stress modelled using a solids viscosity informed by Kinetic theory. The predicted breakup time for a given Ad_η was in good agreement with simulations.

Funding. This research was supported by the Office of Naval Research under Award No. N00014-19-1-2202. The computational resources were provided by the Advanced Research Computing at the University of Michigan, Ann Arbor.

Declaration of interests. The authors report no conflict of interest.

Author ORCIDs.

Yuan Yao <https://orcid.org/0000-0002-4180-1811>;

Jesse Capecelatro <https://orcid.org/0000-0002-1684-4967>.

Appendix A. Sensitivity of aggregate breakup to modelling parameters

Two key metrics used in the analysis of aggregate breakup and model development in the present study are the time-to-breakup, t_{br} , and breakup rate, \dot{N}_c . As summarized in § 2, the numerical prediction of breakup depends on a set of parameters for modelling inelastic collisions and cohesion due to van der Waals forces. The purpose of this appendix is to evaluate the sensitivity of the quantities of interest (QoIs), namely t_{br} and \dot{N}_c , to the various modelling parameters employed. Specific attention is paid to the effect of the spring stiffness, k , and restitution coefficient, e , appearing in (2.8), the role of two-way coupling, the relative importance of fluid torque and choice in cohesion model. The simulation configuration outlined in § 2 is used, with $Re_\lambda = 64$ and $Ad = 0.3$ and 3. It should be noted that although Gu *et al.* (2016) demonstrated previously that simulations of gas-fluidization of cohesive particles are insensitive to the particle stiffness using the modified cohesion model employed here, the present study represents the first application of this model to large (with respect to the Kolmogorov length scale) and dense (near close packing) particle aggregates.

Table 2 summarizes the non-dimensional time-rate-of-breakup and breakup time for different model parameters and conditions, with the values used to generate the results reported in § 3 highlighted in bold. The modified van der Waals model of Gu *et al.* (2016) is also compared with the original model of Hamaker (1937) to demonstrate the reduced dependence of spring stiffness on the QoIs. It can immediately be seen that the QoIs are far more sensitive to the particle stiffness when the original model of Hamaker (1937) is used. Taking the ‘real’ value of particle stiffness to be $k = 7000 \text{ N m}^{-1}$, both models yield the same results when this value is used, albeit with excessively small timesteps. However, as k is reduced to an artificially soft value of 10 N m^{-1} , t_{br}/τ_f changes from 0 to 1750 using Hamaker (1937) with $Ad = 0.3$, whereas t_{br}/τ_f predicted using the modified model remains 0. The QoIs are seen to be even less sensitive to k for higher values of Ad with the modified model. Specifically, varying the stiffness from $k = 7000$ to $k = 10 \text{ N m}^{-1}$ results in a 23.3 % change in breakup rate for $Ad = 0.3$ and only a 0.9 % change for $Ad = 3$. This is likely due to the increased duration of breakup at higher values of Ad . Similar variations in the breakup rate can also be seen when varying the coefficient of restitution, despite it changing from near-elastic ($e = 0.9$) to highly inelastic ($e = 0.1$). Similar trends are observed for the other QoI (t_{br}/τ_f) as well.

The QoIs are found to be much less sensitive to the inclusion of fluid torque. It can be seen that accounting for the fluid torque slightly increases the breakup rate, and has

	<i>Ad</i>	Spring stiffness, <i>k</i> (N m ⁻¹)				Restitution coefficient, <i>e</i>			Two-way coupling		Fluid torque		
		10	100	300	7000	0.1	0.3	0.9	w/	w/o	w/	w/o	
Gu <i>et al.</i> (2016)	$\dot{N}_c \tau_p$	0.3	1523	1219	1246	1167	1371	1167	1523	1523	17 138	1594	1523
		3.0	570	577	565	568	576	568	570	570	10 968	593	570
	t_{br}/τ_f	0.3	0	0	0	0	0	0	0	0	0	0	
		3.0	225	210	280	230	180	210	225	225	0	225	225
Hamaker (1937)	$\dot{N}_c \tau_p$	0.3	914	979	997	1167	826	793	914	914	17 312	937	914
		3.0	0	0	0	568	0	0	0	0	10 765	0	0
	t_{br}/τ_f	0.3	1750	840	800	0	1740	1780	1750	1750	0	1760	1750
		3.0	∞	∞	∞	230	∞	∞	∞	∞	0	∞	∞

Table 2. Breakup time (t_{br}) and time rate of breakup (\dot{N}_c) for different values of model parameters. Values used in the primary study displayed in bold.

negligible effect on the breakup time. For $Ad = 0.3$, the non-dimensional breakup rate $\dot{N}_c \tau_p$ varies from 1523 to 1594, and with $Ad = 3$, it varies from 570 to 593. Meanwhile, it has no noticeable change in the breakup time t_{br} . This is not surprising as fluid torque acting on each particle i , $M_f^{(i)}$, is proportional to the dynamic viscosity μ , which is added to the right-hand side of (2.6) according to (Chen, Li & Marshall 2019)

$$M_f^{(i)} = -\pi \mu d_p^3 (\omega_p^{(i)} - \omega), \tag{A1}$$

where $\omega = \nabla \times \mathbf{u}/2$ is the fluid rotation rate vector. While such effects are known to be important for liquid–solid suspensions, the dynamic viscosity is typically two orders of magnitudes smaller in gas–solid flows. Meanwhile, two-way coupling is seen to have substantial effects on the results.

To obtain a quantitative understanding of how sensitive the QoIs are to the modelling parameters, a variance-based sensitivity analysis is performed. The total-effect Sobol sensitivity indices are computed for each parameter, defined as

$$S_{Ti} = \frac{E_{X_{\sim i}} (Var_{X_i} (Y | X_{\sim i}))}{Var(Y)}, \tag{A2}$$

where Y is the output (QoI), X is a vector of four input parameters (i.e. k , e , two-way coupling, fluid torque), $X_{\sim i}$ denotes the set of all variables except X_i , and E and Var denote the expectation and variance, respectively. Here S_{Ti} can be interpreted as a measure of the contribution of X_i to the output variance, including the total variance caused by its interactions with other input variables, normalized by the global output variance of the QoI, $Var(Y)$. Note that for cases in which the aggregate fails to breakup, $t_{br} = \infty$, which results in ill-defined Sobol indices. To this end, a transformed QoI \hat{t}_{br} is defined to measure the breakup time by monotonically mapping t_{br} to a finite range via

$$\hat{t}_{br} = (t_{br}/\overline{t_{br}})^2 / \left((t_{br}/\overline{t_{br}})^2 + 1 \right) \tag{A3}$$

with $\overline{t_{br}}$ the mean of all finite t_{br} values such that $\hat{t}_{br} = 0$ when $t_{br} = 0$ and $\hat{t}_{br} = 1$ when $t_{br} = \infty$. We found that S_{Ti} is not sensitive to the specific choice of the mapping function as long as it is a monotonic function such that they have the same physical meaning.

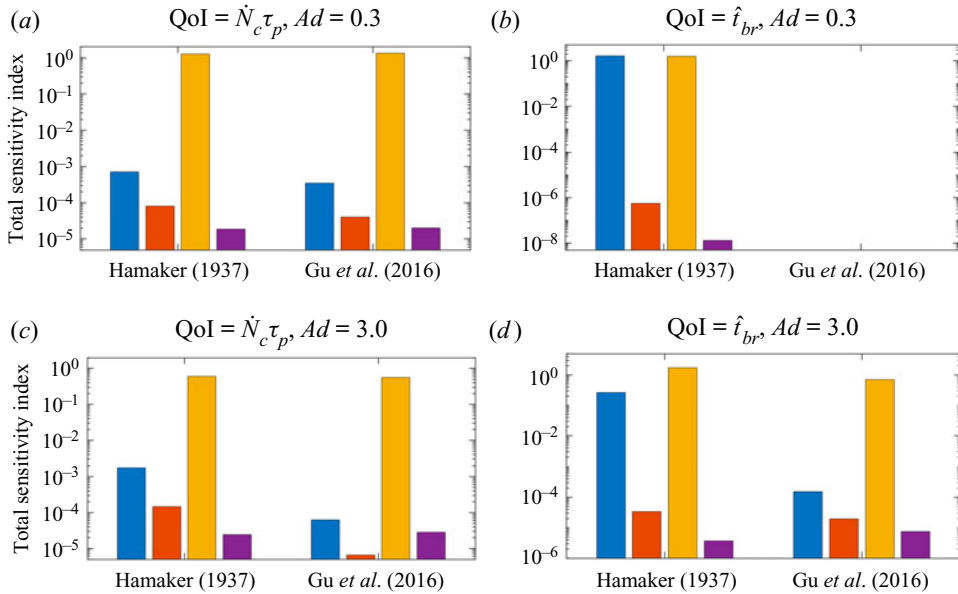


Figure 12. Total-effect Sobol sensitivity index of time-to-breakup (a,c) and breakup rate (b,d) for $Ad = 0.3$ and 3.0 normalized by the global variance of each QoI. Particle stiffness k (blue), restitution coefficient e (orange), two-way coupling (yellow) and the fluid torque (purple).

As shown in figure 12, the modified model of Gu *et al.* (2016) significantly reduces the sensitivity of the particle stiffness on both QoIs. The effect is more profound on $\dot{N}_c \tau_p$ for $Ad = 3$ than $Ad = 0.3$ as previously observed in table 2. For \hat{t}_{br} , however, the dependency on these input parameters are completely removed when $Ad = 0.3$ because the aggregate breaks up instantaneously for all cases. Even when particles are highly cohesive ($Ad = 3$), the Sobol index of k using the model of Gu *et al.* (2016) is approximately three orders of magnitude smaller than Hamaker’s original model, which demonstrates the advantage of using the modified model. Nevertheless, both QoIs are most sensitive to two-way coupling for both values of Ad .

To better illustrate the large discrepancy in QoIs between one-way and two-way coupling, we compare the instantaneous particle distribution and the corresponding flow field at $t/\tau_f = 60$ in figure 13. When one-way coupling is considered, the local flow remains unmodified by the presence of particles, resulting in relatively large interphase slip velocities and consequently large values in drag. It can be seen that despite the presence of cohesion, strong drag induced by the turbulence results in instantaneous breakup. However, with two-way coupling, the near close-packing distribution of particles is seen to result in a no-slip boundary condition, resulting in null drag for all of the particles except those near the surface of the aggregate. In § 3, this was shown to result in fragmentation that occurs progressively from the outer surface where the shear stresses are greatest.

Figure 14 compares the evolution of aggregate breakup using the van der Waals models of Gu *et al.* (2016) and Hamaker (1937). The time-to-breakup and breakup rate are seen to be relatively similar for both values of Ad as k is adjusted using the Gu *et al.* model. However for the original Hamaker model, larger values of k results in significantly larger breakup time when $Ad = 0.3$, and fails to predict breakup when $Ad = 3$, which confirms that the particle dynamics are highly sensitive to particle stiffness using the original Hamaker model. Note that although the dependency of k is not removed completely as

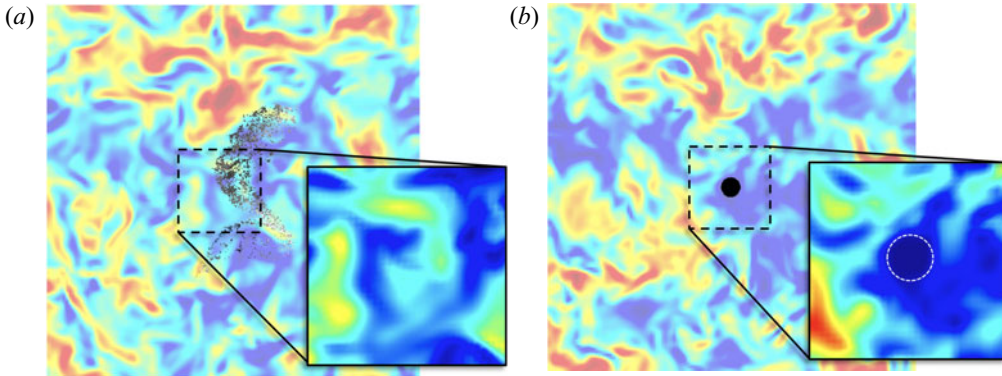


Figure 13. Comparison of the velocity field and particle distribution with (a) one-way coupling and (b) two-way coupling for $Re_\lambda = 64$ and $Ad = 3$ at $t/\tau_f = 60$. Colour scheme is the same as figure 1 with white dashed line showing the aggregate interface.

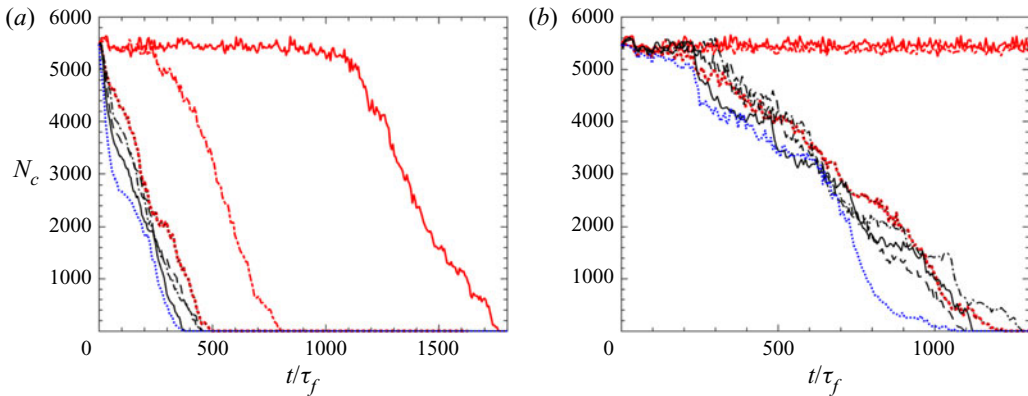


Figure 14. Evolution of the number of particles within the aggregate for (a) $Ad = 0.3$ and (b) $Ad = 3$ with $Re_\lambda = 64$. van der Waals model of Gu *et al.* 2016 (black) and Hamaker 1937 (red) with $k = 10$ (—), 100 (---), 300 (· · ·) and 7000 (· · ·) $N\ m^{-1}$. JKR theory (which is independent of k) (blue).

shown in figure 12, the sensitivity is relatively small and the model of breakup proposed herein is anticipated to apply generally for dense spherical aggregates.

Recall that treating inter-particle collisions and cohesion as additive forces implicitly assumes the surface profile of the particles remain unmodified according to the DMT theory (Derjaguin *et al.* 1975). For solid particles in air, this assumption is typically only valid for submicrometre-size particles. For larger particles, the JKR theory might be more appropriate, which assumes that adhesion occurs only within the flattened contact region, and consequently the collision force is nonlinearly coupled with the adhesion force. The validity of each theory is characterized by the Tabor number (2.7). DMT is most appropriate when $\lambda_T \ll 1$ (typically $\lambda_T \lesssim 0.1$) and the JKR model is valid when $\lambda_T \gg 1$ (typically $\lambda_T \gtrsim 10$). As discussed in § 2, $0.19 \leq \lambda_T \leq 0.98$, and thus DMT was chosen in the present study. In order to show the applicability of the DMT theory in the cases considered here, the aggregate breakup processes using both theories are compared in figure 14 for $Ad = 0.3$ and 3. The DMT theory is analysed by coupling the soft-sphere collision model with the cohesion model of Gu *et al.* (2016) in addition to the original van der Waals model of Hamaker (1937). The numerical implementation of JKR model

is based on Chen *et al.* (2019). For both values of Ad , the JKR model predicts a slightly larger rate of breakup than the DMT models ($\dot{N}_c \tau_p = 1610$ versus 1523 for $Ad = 0.3$ and 598 versus 570 for $Ad = 3$), and the breakup times are in reasonable agreement for all cases ($t_{br}/\tau_f = 0$ versus 0 for $Ad = 0.3$ and 220 versus 225 for $Ad = 3$).

REFERENCES

- ANDERSON, T.B. & JACKSON, R. 1967 Fluid mechanical description of fluidized beds. Equations of motion. *Ind. Engng Chem. Fundam.* **6** (4), 527–539.
- BÄBLER, M.U., MORBIDELLI, M. & BALDYGA, J. 2008 Modelling the breakup of solid aggregates in turbulent flows. *J. Fluid Mech.* **612**, 261–289.
- BACHE, D.H. 2004 Floc rupture and turbulence: a framework for analysis. *Chem. Engng Sci.* **59** (12), 2521–2534.
- BATCHO, P.F., MOLLER, J.C., PADOVA, C. & DUNN, M.G. 1987 Interpretation of gas turbine response due to dust ingestion. *ASME: J. Engng Gas Turbines Power* **109**, 344–352.
- BEGAT, P., MORTON, D.A.V., STANIFORTH, J.N. & PRICE, R. 2004 The cohesive-adhesive balances in dry powder inhaler formulations II: influence on fine particle delivery characteristics. *Pharmaceut. Res.* **21** (10), 1826–1833.
- BOCQUET, L., LOSERT, W., SCHALK, D., LUBENSKY, T.C. & GOLLUB, J.P. 2001 Granular shear flow dynamics and forces: experiment and continuum theory. *Phys. Rev. E* **65** (1), 011307.
- BONS, J.P., PRENTER, R. & WHITAKER, S. 2017 A simple physics-based model for particle rebound and deposition in turbomachinery. *Trans. ASME: J. Turbomach.* **139** (8), 081009.
- BREUER, M. & ALMOHAMMED, N. 2015 Modeling and simulation of particle agglomeration in turbulent flows using a hard-sphere model with deterministic collision detection and enhanced structure models. *Intl J. Multiphase Flow* **73**, 171–206.
- CAPECELATRO, J. & DESJARDINS, O. 2013 An Euler–Lagrange strategy for simulating particle-laden flows. *J. Comput. Phys.* **238**, 1–31.
- CAPECELATRO, J., PEPIOT, P. & DESJARDINS, O. 2014 Numerical characterization and modeling of particle clustering in wall-bounded vertical risers. *Chem. Engng J.* **245**, 295–310.
- CHEN, S. & LI, S. 2020 Collision-induced breakage of agglomerates in homogenous isotropic turbulence laden with adhesive particles. [arXiv:2004.09726](https://arxiv.org/abs/2004.09726).
- CHEN, S., LI, S. & MARSHALL, J.S. 2019 Exponential scaling in early-stage agglomeration of adhesive particles in turbulence. *Phys. Rev. Fluids* **4** (2), 024304.
- COCCO, R., SHAFFER, F., HAYS, R., KARRI, S.B.R. & KNOWLTON, T. 2010 Particle clusters in and above fluidized beds. *Powder Technol.* **203** (1), 3–11.
- CUNDALL, P.A. & STRACK, O.D.L. 1979 A discrete numerical model for granular assemblies. *Gèotechnique* **29** (1), 47–65.
- DERJAGUIN, B.V., MULLER, V.M. & TOPOROV, YU.P. 1975 Effect of contact deformations on the adhesion of particles. *J. Colloid Interface Sci.* **53** (2), 314–326.
- DESJARDINS, O., BLANQUART, G., BALARAC, G. & PITSCH, H. 2008 High order conservative finite difference scheme for variable density low Mach number turbulent flows. *J. Comput. Phys.* **227** (15), 7125–7159.
- DIZAJI, F.F. & MARSHALL, J.S. 2017 On the significance of two-way coupling in simulation of turbulent particle agglomeration. *Powder Technol.* **318**, 83–94.
- DIZAJI, F.F., MARSHALL, J.S. & GRANT, J.R. 2019 Collision and breakup of fractal particle agglomerates in a shear flow. *J. Fluid Mech.* **862**, 592–623.
- DUNN, M.G., BARAN, A.J. & MIATECH, J. 1996 Operation of gas turbine engines in volcanic ash clouds. *ASME: J. Engng Gas Turbines Power* **118**, 724–731.
- FANELLI, M., FEKE, D.L. & MANAS-ZLOCZOWER, I. 2006a Prediction of the dispersion of particle clusters in the nano-scale—Part II: unsteady shearing responses. *Chem. Engng Sci.* **61** (15), 4944–4956.
- FANELLI, M., FEKE, D.L. & MANAS-ZLOCZOWER, I. 2006b Prediction of the dispersion of particle clusters in the nano-scale—Part I: steady shearing responses. *Chem. Engng Sci.* **61** (2), 473–488.
- FLESCH, J.C., SPICER, P.T. & PRATSINIS, S.E. 1999 Laminar and turbulent shear-induced flocculation of fractal aggregates. *AIChE J.* **45** (5), 1114–1124.
- FORSYTH, P.R., GILLESPIE, D.R.H. & MCGILVRAY, M. 2018 Development and applications of a coupled particle deposition–dynamic mesh morphing approach for the numerical simulation of gas turbine flows. *Trans. ASME: J. Engng Gas Turbines Power* **140** (2), 022603.
- FRIEDLANDER, S.K. 2000 *Smoke, Dust, and Haze*, vol. 198. Oxford University Press.

Deagglomeration of cohesive particles by turbulence

- GRANT, G. & TABAKOFF, W. 1975 Erosion prediction in turbomachinery resulting from environmental solid particles. *J. Aircraft* **12** (5), 471–478.
- GU, Y., OZEL, A. & SUNDARESAN, S. 2016 A modified cohesion model for CFD–DEM simulations of fluidization. *Powder Technol.* **296**, 17–28.
- HAMAKER, H.C. 1937 The London—van der Waals attraction between spherical particles. *Physica* **4** (10), 1058–1072.
- HAMED, A., TABAKOFF, W.C. & WENGLARZ, R.V. 2006 Erosion and deposition in turbomachinery. *J. Propul. Power* **22** (2), 350–360.
- HIGASHITANI, K., IIMURA, K. & SANDA, H. 2001 Simulation of deformation and breakup of large aggregates in flows of viscous fluids. *Chem. Engng Sci.* **56** (9), 2927–2938.
- HO, C.A. & SOMMERFELD, M. 2002 Modelling of micro-particle agglomeration in turbulent flows. *Chem. Engng Sci.* **57** (15), 3073–3084.
- VAN DER HOEF, M.A., VAN SINT ANNALAND, M., DEEN, N.G. & KUIPERS, J. 2008 Numerical simulation of dense gas-solid fluidized beds: a multiscale modeling strategy. *Annu. Rev. Fluid Mech.* **40**, 47–70.
- JARVIS, P., JEFFERSON, B., GREGORY, J. & PARSONS, S.A. 2005 A review of floc strength and breakage. *Water Res.* **39** (14), 3121–3137.
- JOHNSON, K.L. & GREENWOOD, J.A. 1997 An adhesion map for the contact of elastic spheres. *J. Colloid Interface Sci.* **192** (2), 326–333.
- JOHNSON, K.L., KENDALL, K. & ROBERTS, A.D. 1971 Surface energy and the contact of elastic solids. *Proc. R. Soc. Lond. A* **324** (1558), 301–313.
- KOSINSKI, P. & HOFFMANN, A.C. 2010 An extension of the hard-sphere particle–particle collision model to study agglomeration. *Chem. Engng Sci.* **65** (10), 3231–3239.
- KOUSAKA, Y., OKUYAMA, K., SHIMIZU, A. & YOSHIDA, T. 1979 Dispersion mechanism of aggregate particles in air. *J. Chem. Engng Japan* **12** (2), 152–159.
- LIU, L.F., ZHANG, Z.P. & YU, A.B. 1999 Dynamic simulation of the centripetal packing of mono-sized spheres. *Physica A* **268** (3–4), 433–453.
- LIU, P. & HRENYA, C.M. 2018 Cluster-induced deagglomeration in dilute gravity-driven gas-solid flows of cohesive grains. *Phys. Rev. Lett.* **121** (23), 238001.
- LUNDGREN, T.S. 2003 Linearly forced isotropic turbulence. *Tech. Rep.* 461–473. Center for Turbulence Research.
- MAHECHA-BOTERO, A., GRACE, J.R., ELNASHAIE, S. & LIM, C.J. 2009 Advances in modeling of fluidized-bed catalytic reactors: a comprehensive review. *Chem. Engng Commun.* **196** (11), 1375–1405.
- MALLOUPPAS, G., GEORGE, W.K. & VAN WACHEM, B.G.M. 2013 New forcing scheme to sustain particle-laden homogeneous and isotropic turbulence. *Phys. Fluids* **25** (8), 083304.
- MARSHALL, J.S. 2009 Discrete-element modeling of particulate aerosol flows. *J. Comput. Phys.* **228** (5), 1541–1561.
- MARSHALL, J.S. & LI, S. 2014 *Adhesive Particle Flow*. Cambridge University Press.
- MCCAVE, I.N. 1984 Erosion, transport and deposition of fine-grained marine sediments. *Geol. Soc. Lond. Spec. Publ.* **15** (1), 35–69.
- MIKAMI, T., KAMIYA, H. & HORIO, M. 1998 Numerical simulation of cohesive powder behavior in a fluidized bed. *Chem. Engng Sci.* **53** (10), 1927–1940.
- MOUSEL, J.A. & MARSHALL, J.S. 2010 Aggregate growth and breakup in particulate suspension flow through a micro-nozzle. *Microfluid. Nanofluid.* **8** (2), 171–186.
- PAN, H., CHEN, X.-Z., LIANG, X.-F., ZHU, L.-T. & LUO, Z.-H. 2016 CFD simulations of gas–liquid–solid flow in fluidized bed reactors—a review. *Powder Technol.* **299**, 235–258.
- PANDYA, J.D. & SPIELMAN, L.A. 1983 Floc breakage in agitated suspensions: effect of agitation rate. *Chem. Engng Sci.* **38** (12), 1983–1992.
- PIERCE, C.D. 2001 Progress-variable approach for large-eddy simulation of turbulent combustion. PhD thesis, Citeseer.
- ROY, S., LUDING, S. & WEINHART, T. 2017 A general (ized) local rheology for wet granular materials. *New J. Phys.* **19** (4), 043014.
- RUAN, X., CHEN, S. & LI, S. 2020 Structural evolution and breakage of dense agglomerates in shear flow and Taylor–Green vortex. *Chem. Engng Sci.* **211**, 115261.
- RYBALKO, M., LOTH, E. & LANKFORD, D. 2012 A Lagrangian particle random walk model for hybrid RANS/LES turbulent flows. *Powder Technol.* **221**, 105–113.
- SACCO, C., BOWEN, C., LUNDGREEN, R., BONIS, J.P., RUGGIERO, E., ALLEN, J. & BAILEY, J. 2018 Dynamic similarity in turbine deposition testing and the role of pressure. *Trans. ASME: J. Engng Gas Turbines Power* **140** (10), 102605.

- SONNTAG, R.C. & RUSSEL, W.B. 1987 Structure and breakup of flocs subjected to fluid stresses: II. Theory. *J. Colloid Interface Sci.* **115** (2), 378–389.
- SUN, R., XIAO, H. & SUN, H. 2018 Investigating the settling dynamics of cohesive silt particles with particle-resolving simulations. *Adv. Water Resour.* **111**, 406–422.
- SYAMLAL, M., ROGERS, W. & O'BRIEN, T.J. 1993 Mfix documentation theory guide. *Tech. Rep.* USDOE Morgantown Energy Technology Center, WV (United States).
- TAYLOR, G.I. 1949 The shape and acceleration of a drop in a high speed air stream. *Collected Papers III*. pp. 457–464.
- TENNETI, S., GARG, R. & SUBRAMANIAM, S. 2011 Drag law for monodisperse gas–solid systems using particle-resolved direct numerical simulation of flow past fixed assemblies of spheres. *Intl J. Multiphase Flow* **37** (9), 1072–1092.
- UHLMANN, M. 2008 Interface-resolved direct numerical simulation of vertical particulate channel flow in the turbulent regime. *Phys. Fluids* **20** (5), 053305.
- VO, T.-T., MUTABARUKA, P., NEZAMABADI, S., DELENNE, J.-Y. & RADJAI, F. 2020 Evolution of wet agglomerates inside inertial shear flow of dry granular materials. *Phys. Rev. E* **101**, 032906.
- VOWINCKEL, B., BIEGERT, E., LUZZATTO-FEGIZ, P. & MEIBURG, E. 2019a Consolidation of freshly deposited cohesive and noncohesive sediment: particle-resolved simulations. *Phys. Rev. Fluids* **4** (7), 074305.
- VOWINCKEL, B., WITHERS, J., LUZZATTO-FEGIZ, P. & MEIBURG, E. 2019b Settling of cohesive sediment: particle-resolved simulations. *J. Fluid Mech.* **858**, 5–44.
- VAN WACHEM, B., THALBERG, K., NGUYEN, D., DE JUAN, L.M., REMMELGAS, J. & NIKLASSON-BJORN, I. 2020 Analysis, modelling and simulation of the fragmentation of agglomerates. *Chem. Engng Sci.* **227**, 115944.
- WANG, F.-J., ZHU, J.-X. & BEECKMANS, J.M. 2000 Pressure gradient and particle adhesion in the pneumatic transport of cohesive fine powders. *Intl J. Multiphase Flow* **26** (2), 245–265.
- WEILER, C., WOLKENHAUER, M., TRUNK, M. & LANGGUTH, P. 2010 New model describing the total dispersion of dry powder agglomerates. *Powder Technol.* **203** (2), 248–253.
- WENGELER, R. & NIRSCHE, H. 2007 Turbulent hydrodynamic stress induced dispersion and fragmentation of nanoscale agglomerates. *J. Colloid Interface Sci.* **306** (2), 262–273.
- WHITAKER, S.M., PRENTER, R. & BONS, J.P. 2015 The effect of freestream turbulence on deposition for nozzle guide vanes. *Trans. ASME: J. Turbomach.* **137** (12), 121001.
- YANG, J., WU, C.-Y. & ADAMS, M. 2013 DEM analysis of particle adhesion during powder mixing for dry powder inhaler formulation development. *Granul. Matt.* **15** (4), 417–426.
- YANG, J., WU, C.-Y. & ADAMS, M. 2015 Numerical modelling of agglomeration and deagglomeration in dry powder inhalers: a review. *Curr. Pharm. Design* **21** (40), 5915–5922.
- YAO, Y. & CAPECELATRO, J. 2018 Competition between drag and Coulomb interactions in turbulent particle-laden flows using a coupled-fluid–Ewald-summation based approach. *Phys. Rev. Fluids* **3** (3), 034301.
- YAO, Y. & CAPECELATRO, J. 2019 Electrohydrodynamic generation of atmospheric turbulence. *Phys. Rev. Fluids* **4** (12), 123701.
- ZEIDAN, M., XU, B.H., JIA, X. & WILLIAMS, R.A. 2007 Simulation of aggregate deformation and breakup in simple shear flows using a combined continuum and discrete model. *Chem. Engng Res. Des.* **85** (12), 1645–1654.
- ZHAO, K., VOWINCKEL, B., HSU, T.-J., KÖLLNER, T., BAI, B. & MEIBURG, E. 2020 An efficient cellular flow model for cohesive particle flocculation in turbulence. *J. Fluid Mech.* **889**, R3.